Solar Phys (2011) 268: 175–193
DOI 10.1007/s11207-010-9669-2

Gamma-Ray and High-Energy-Neutron Measurements on CORONAS-F during the Solar Flare of 28 October 2003

Sergei N. Kuznetsov · Victoria G. Kurt · Boris Y. Yushkov · Karel Kudela · Vladimir I. Galkin

Received: 30 November 2007 / Accepted: 2 November 2010 / Published online: 30 November 2010

Abstract The solar flare of 28 October 2003 (X17.2/4B) was recorded by the SONG instrument onboard the CORONAS-F satellite. A description of the SONG instrument, its in-orbit operation and the principal data reduction methods used to derive the flare gamma-ray properties are presented. Appreciable gamma-ray emission was observed in the 0.2 – 300 MeV energy range. Several time intervals were identified which showed major changes in the intensity and spectral shape of the flare gamma-ray emission. The primary bremsstrahlung proves to be extended to 90 MeV and dominates during 11:02:11 – 11:03:50 UT time interval, *i.e.* at the beginning of the flare impulsive phase. Afterwards, the SONG response was consistent with detection of the pion-decay gamma emission. A sharp increase in the pion-decay-generated gamma-ray emission was observed at $11:03:51 \pm 2$ s UT, implying a substantial change in the spectrum of accelerated ions, which testified the appearance of protons with energies of > 300 MeV on the Sun. This emission lasted at least 8 – 9 min until the end of our measurements. The ion acceleration to high energies was also proved by the detection of neutrons with energies > 500 MeV. It was found that the most efficient acceleration of high-energy protons coincides in time with the highest rate of the magnetic-flux change rate. The maximum gamma-ray flux at 100 MeV was 1.1×10^{-2} photons cm^{-2} s^{-1} MeV^{-1}, exceeding all the fluxes that have ever been recorded.

1. Introduction

Observation of the gamma-ray emission from solar flares is among the most important ways to explore the processes of electron and ion acceleration. Gamma rays from several major solar flares observed in October and November 2003 provided evidence for the presence of high-energy nuclei and electrons in the solar atmosphere (Veselovsky *et al.*, 2004;

S.N. Kuznetsov is deceased.

S.N. Kuznetsov · V.G. Kurt · B.Y. Yushkov (✉) · V.I. Galkin
Skobeltsyn Institute of Nuclear Physics, Moscow State University, Moscow 119991, Russia
e-mail: clef@srd.sinp.msu.ru

K. Kudela
Institute of Experimental Physics, Slovak Academy of Science, Kosice 04353, Slovakia

Kuznetsov *et al.*, 2005a, 2008a; Share *et al.*, 2004; Gros *et al.*, 2004; Kurt *et al.*, 2009, 2010). The appearance of relativistic particles near the Earth was detected from space (Kuznetsov *et al.*, 2008b; http://spidr.ngdc.noaa.gov/spidr/) and by the neutron monitor (NM) network (*e.g.* Plainaki *et al.*, 2005; Bieber *et al.*, 2005; http://helios.izmiran.rssi.ru/cosray/main.html).

Four gamma-ray-emission events with high energies were recorded by the SONG (SOlar Neutrons and Gamma-rays) instrument onboard CORONAS-F (*Complex ORbital ObservatioNs of the Active Sun*) on 26, 28, and 29 October and on 4 November 2003. The flare of 28 October was the one observed best among all of them. The ground-based measurements (Miroshnichenko *et al.*, 2005; Nonaka *et al.*, 2006) indicated that protons were accelerated in this flare to energies of about 10 GeV, with a spectral slope of $\sim 3-3.5$. In this paper, we discuss both gamma-ray and neutron observations of this flare, with special emphasis on high-energy gamma-ray emission. The gamma-ray spectrum gives evidence for the presence of neutral pions, which require accelerated protons with kinetic energies of ~ 300 MeV or higher. The development of the flare observed in gamma-ray emission consists of two phases. The first, 'impulsive' phase can be subdivided into two time intervals. The first interval (A) exhibits a continuum attributable to the primary-electron bremsstrahlung extending from about 20 keV to 90 MeV or higher, narrow gamma lines observed by INTEGRAL/SPI (Gros *et al.*, 2004; Kiener *et al.*, 2006), and signs of pion production. The 2.223-MeV line formed by neutrons captured by hydrogen was also observed during this phase by SONG and by INTEGRAL. The second, interval B exhibits a sharp increase of the 2.223-MeV line intensity as well as of prompt lines, and strong evidence for pion production. The second, 'extended' phase (C), or decay phase of the pion-produced and gamma-line emission lasted at least $7-8$ min until the end of our measurements, with a weak sign of variability. The intrinsic properties of the gamma-ray emission of the 28 October flare are similar to the corresponding characteristics of several other major flares (see *e.g.* Debrunner *et al.*, 1983, 1997; Forrest *et al.*, 1985; Chupp *et al.*, 1987; Rieger, 1989; Akimov *et al.*, 1991, 1994, 1996; Kurt, Akimov, and Leikov, 1996; Kurt *et al.*, 2009, 2010; Dunphy *et al.*, 1999; Vilmer *et al.*, 2003; Kuznetsov *et al.*, 2006b, 2008a; Grechnev *et al.*, 2008).

The paper is organized as follows: Section 2 describes the SONG instrument and its in-flight calibration; Section 3 describes the observations of the flare of 28 October 2003; Section 3.1 describes time profiles of the gamma-ray emission including the routine of background subtraction; Section 3.2 describes the dynamics of the gamma-ray-emission spectrum; Section 3.3 describes the neutron measurements; Section 4 presents our results and discussion.

2. Description of the SONG Instrument

The SONG instrument (see Figure 1) was developed for a joint experiment of SINP MSU (Moscow) and IEP SAS (Kosice). The detector had a CsI(Tl) crystal with a diameter of 20 cm and a height of 10 cm surrounded by a plastic scintillator shield (Kuznetsov *et al.*, 2002, 2004). The front plastic counter had a thickness of 1 cm. The thickness of the side/back plastic counter was 2 cm. Charged-particle rejection in neutron and photon measurements was based on the veto signals obtained from the two plastic counters. A veto signal corresponded to an energy deposition in the plastic scintillator higher than 0.3 MeV. The gamma-emission detection channels were formed by pulse-height discriminators with thresholds of 28, 53, 150, and 500 keV and 1.3, 4.0, 7.0, 15, 26, 41, 60, 100, and 200 MeV. These discriminators were also used for neutron- and electron-flux measurements.

In the absence of an anticoincidence pulse of the plastic counters due to a charged particle, each of the output pulses from the discriminators was recorded in a gamma channel. In

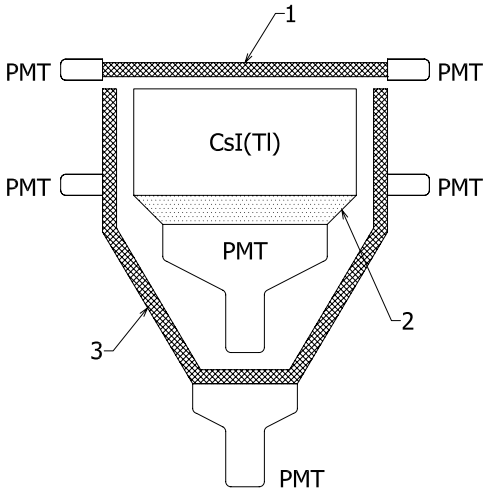

Figure 1 A schematic of the SONG instrument. The locations of the front plastic counter (1), the light guide (2), and the side and back plastic counters (3) are shown (PMT stands for 'photomultiplier tube').

addition, the pulses in the energy range of 1 – 100 MeV accompanied by the 'neutron' master were recorded in 'neutron' channels. The pulses associated with the gamma-ray emission in the energy range 0.4 – 12 MeV were also processed by a 240-channel quasi-logarithmic pulse-height analyzer.

Neutrons with energies >20 MeV produce recoil protons and other heavy non-relativistic particles in a CsI(Tl) crystal, whereas gamma photons produce relativistic electrons. The intensity ratio of the fast ($\tau = 0.5 - 0.7$ μs) and slow ($\tau \sim 7$ μs) components of the scintillation pulses in the CsI(Tl) crystal depends on the particle's ionizing power, which in turn is different for relativistic electrons and slow heavy particles. This allows for discrimination between neutrons and gamma photons (Bogomolov *et al.*, 1996). Secondary particles produced by neutrons have a wide energy distribution below the energy of incident neutron. Therefore, the energy of a neutron cannot be determined from its energy deposition. The effective area of SONG for the neutron detection varies with the neutron energy. It reaches its maximum of 30 – 32 cm^2 at energies of 100 – 200 MeV and falls down to zero at $E \approx 800$ MeV (Panasyuk *et al.*, 2001). This decrease is due to the escape of secondary charged particles from the CsI(Tl) crystal and their subsequent detection by the back anticoincidence plastic counter.

A ground-based calibration of the SONG pulse-height discriminators was made using radioactive sources Cs^{137} (662 keV) and Co^{60} (1.17 and 1.33 MeV) and secondary cosmic-ray muons. In the latter case, an additional counter was mounted above the crystal and set in a coincidence mode to detect only the vertically moving muons. These muons are relativistic particles, and their energy deposition in the CsI(Tl) crystal is about 90 MeV. We calibrated the electric thresholds of the channels using these energy points with the assumption of a linear energy-amplitude dependence. These calibrations did not provide an absolute response function at high energies.

The SONG instrument did not contain any in-flight calibration devices. The stability of the detector was estimated using in-flight data. Figure 2 presents the integral spectra of the gamma radiation averaged over many orbits in August 2001 and in October 2003 near the geomagnetic equator (cutoff rigidities >10 GV) under quiet geomagnetic conditions. Variations of the background gamma-ray fluxes in this region are small (see *e.g.* Harris, Share, and Leising, 2003), because they are determined by the primary high-energy (>15 GeV) cosmic rays, which have virtually constant fluxes during the solar activity cycle. Thus, we

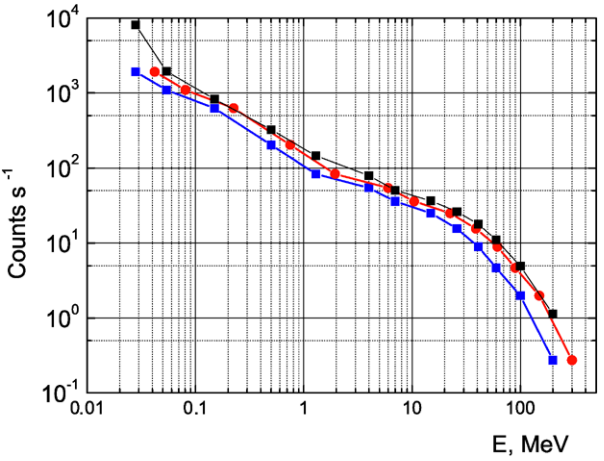

Figure 2 The integral spectra of gamma-ray radiation recorded by the SONG instrument in the geomagnetic-equator region in August 2001 (black curve) and in October 2003 (blue curve). The red curve represents the latter spectrum corrected by multiplying the energy thresholds by a factor 1.5.

can account for the observed change of the count rates of the background gamma-ray emission by a shift of the detector parameters. We also evaluated the channel thresholds. We believe that the two measured background spectra would coincide if the nominal threshold values were corrected for October 2003, multiplying by a factor of 1.5 ± 0.1 (see Figure 2). The energy dependence of the SONG efficiency was taken into account in our calculation. From here on, we will use the corrected threshold values, which are equal to the nominal ones multiplied by the factor of 1.5.

3. Observations

The CORONAS-F satellite operated in a near-Earth circular orbit (initial altitude $\sim$ 500 km, inclination 82.5°) from August 2001 to December 2005. One of the satellite's axes was kept oriented toward the Sun and the viewing direction of the SONG detector was parallel to this axis. The SONG instrument collected data nearly continuously during each 93-min orbit. Kuznetsov *et al.* (2003a, 2003b, 2006a) and Bogomolov *et al.* (2003) described observations of solar flares by SONG in 2001 – 2004.

It was found during the satellite flight that the count rates of the SONG channels depended slightly on variations in the solar wind velocity V_{sw} and interplanetary magnetic field (IMF) when the satellite was located in the polar cap regions in the absence of solar gamma-ray emission and solar energetic particles. Table 1 and Figure 3 present an overview of the local conditions during our measurements and the count rates of several SONG channels for the time interval 07:30 – 12:00 UT on 28 October 2003. They demonstrate that the values of the IMF, V_{sw} and solar wind density, N_{sw}, were virtually constant, as the geomagnetic activity indices during the time interval 08 – 12 UT. The B_z component of the IMF, which can affect the magnetosphere, did not exceed 5 nT during the time interval 10 – 12 UT. Consequently, there were no IMF variations that could initiate any short-term geomagnetic-field disturbances. This suggests that the cutoff rigidity in the polar cap region was not affected by the previous solar activity during the observation time of the 28 October 2003 flare.

According to the logic of the experiment, the count rates of the gamma-ray channels were the sums of photon and neutron events. However, it can be clearly seen in Figure 3 that these count rates were always 100 times higher than the count rates in the neutron channels, even during the short time interval when SONG detected the neutrons.

Table 1 Observational conditions for the flare of 28 October 2003

UT, h	B_Z, nT	N_{sw}, cm^{-3}	V_{sw}, $km\,s^{-1}$	K_p	D_{st}, nT
8 – 9	−4.2	7	613	3^+	−29
9 – 10	7.2	4	654	4^+	−48
10 – 11	4.8	1.3	759	4^+	−47
11 – 12	4.0	1.6	768	4^+	−39

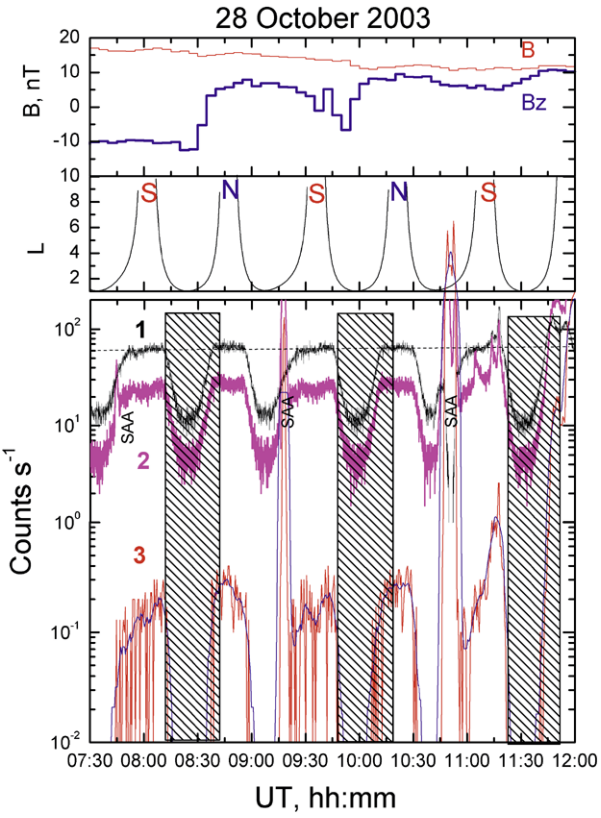

Figure 3 Overview of the SONG measurements on 28 October 2003: IMF and its B_Z component (top panel); the McIlwain parameter L of the CORONAS-F orbital points (middle panel; N and S indicate the Northern and Southern polar caps). Bottom panel represents the count rates of protons with $E_p = 300 – 400$ MeV (1), gamma-rays with $E\gamma = 60 – 90$ MeV (2), and neutrons with energy depositions of 40 – 60 MeV (red curve 3, blue curve corresponding to the smoothed count-rate values for the same neutrons). The time intervals of the Sun occultation by the Earth are shaded. SAA denotes the South Atlantic anomaly region.

The CORONAS-F passage through the southern Earth's polar cap at an altitude of 440 km began at 11:02 UT after crossing the outer *radiation belt* (RB). An increase in the gamma-ray count rate observed during this crossing was due to the bremsstrahlung produced by RB electrons. The satellite entering the Earth's shadow at 11:21:20 UT ceased the solar-emission measurements. Therefore, we had almost 20 minutes to observe the flare gamma-ray emission and the onset of the high-energy particle flux. Figure 4 shows the relative response of the SONG crystal and shield systems, which directly allowed a classification to be made of the observed transients in most cases between 11:02 and 11:12:30 UT. For example, the apparent enhancements with onset times of 11:12:30 and 11:17:30 UT were caused by the arrivals of energetic solar protons. The sharp count-rate decay near 11:20 UT was due to an increase in the geomagnetic cutoff value. Further, we will present the SONG data from the high-energy X-ray, gamma-ray, and neutron channels.

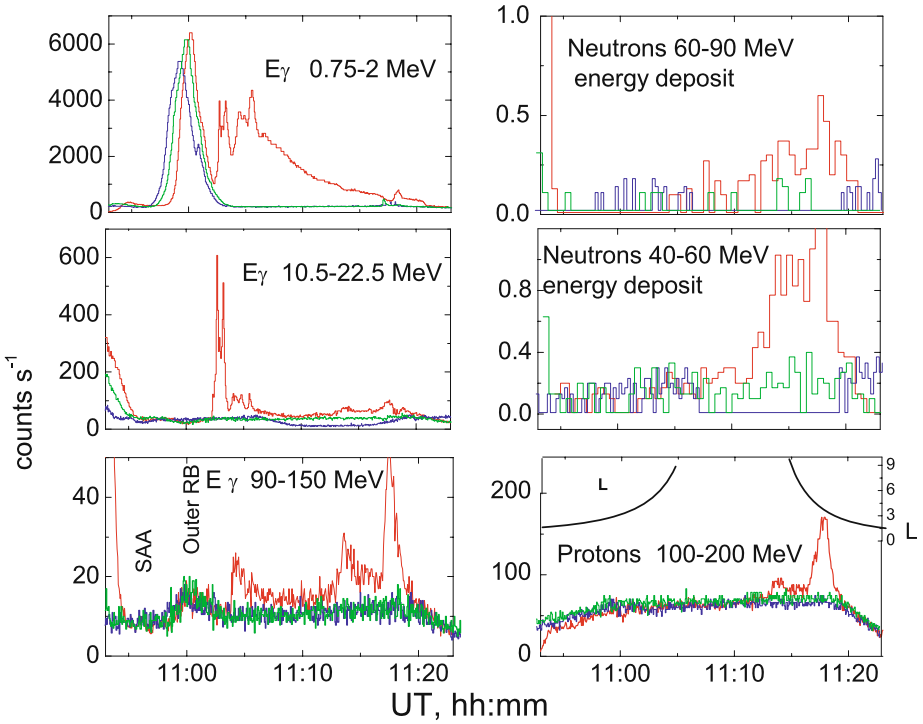

Figure 4 Comparison between the SONG measurements during the solar flare and in the previous orbits. The green and blue curves mark the background data time-shifted to the orbit during which the flare occurred. The red curves correspond to the flare orbit.

3.1. Time Profiles of the Gamma-Ray Emission

The X17.2/4B flare occurred in NOAA Active Region 10486 at a heliographic position of 16°S, 08°E on 28 October 2003 and lasted long. It was observed in the soft X-ray and Hα-emission from 09:40 to 18:00 UT. The commencement of the impulsive phase of the flare was found to be 11:01 – 11:02 UT according to measurements in various wavelengths (Kuznetsov *et al.*, 2005a; Gros *et al.*, 2004; http://spidr.ngdc.noaa.gov/spidr/; Trottet *et al.*, 2008; Miklenic, Veronig, and Vršnak, 2009a, 2009b). The extrapolation of the shock-wave and CME trajectories back to the Sun permitted us to estimate their lift-off time as 11:01:39 UT ± 30 s (Kuznetsov *et al.*, 2005a; http://cdaw.gsfc.nasa.gov). Thus, we can assume with high confidence that the onset time of the main flare energy release was between 11:01 and 11:02 UT.

Figure 5 shows the response of the SONG detector to the X-ray and gamma emission of the flare over the range of energy losses from 0.23 to 300 MeV. An overload of telemetry digital counters was observed between 11:02 and 11:06 UT in two low-energy channels (42 – 80 and 80 – 225 keV), which are not represented in this figure. The net count rates due to the flare (4-s time bins) were obtained by subtracting the background count rates averaged over five previous crossings of the same polar cap. Longer-time averaging is not suitable, because the flare of 28 October was preceded by the flare of 26 October, which produced varying high-level fluxes of charged particles in interplanetary space and in the polar caps (see *e.g.* Veselovsky *et al.*, 2004; Mewaldt *et al.*, 2005). A significant flare contribution to

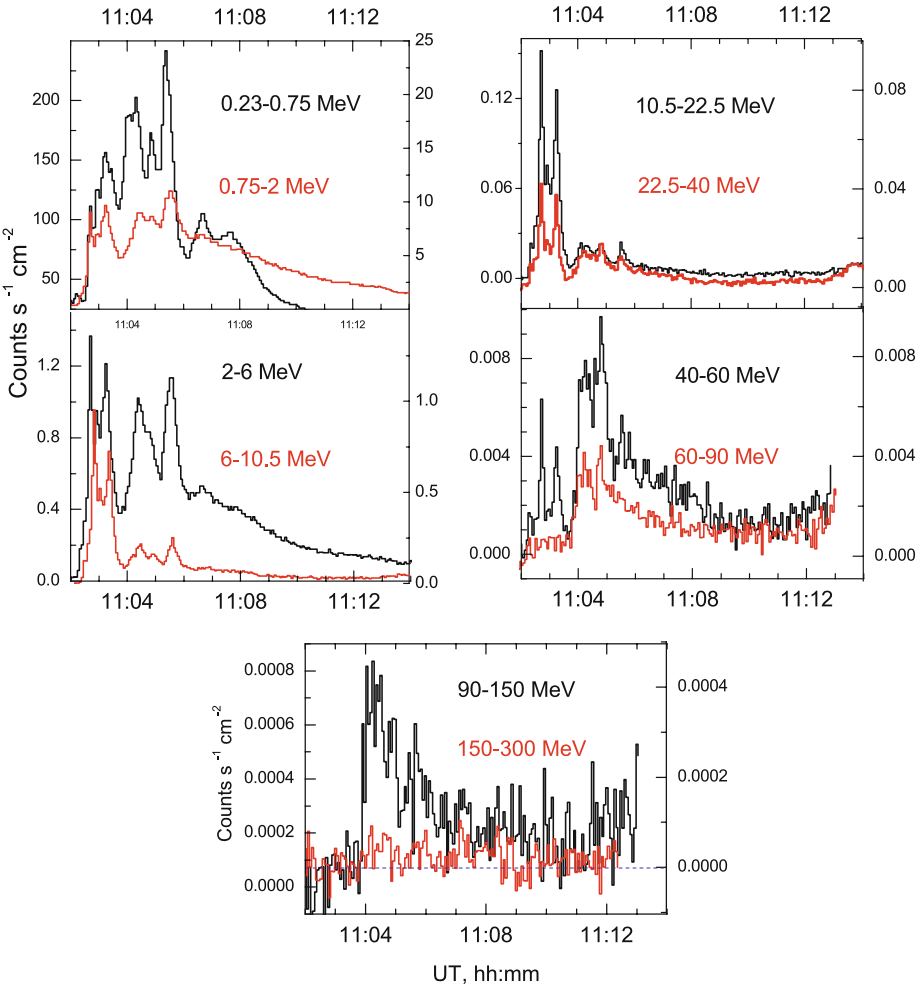

Figure 5 Time evolution of the response of SONG during the flare of 28 October 2003. The background count rates are subtracted. The left ordinate axis in each panel corresponds to the lower energy channel, the right axis to the higher energy one.

the count rates in X-ray and gamma-ray channels of the SONG was recorded from 11:02:11 to 11:12:30 UT. During the same time interval, the MKL instrument that operated onboard CORONAS F (Kuznetsov *et al.*, 2005b) did not detect any sharp increases in the fluxes of electrons with energies 0.3 – 3 MeV and protons with energies 1 – 5 MeV. Therefore, we are certain that the background level during the flare observation time did not vary. The selection of flare gamma-ray photons was no longer unambiguous after 11:12:30 UT, when the bulk of the flare charged particles arrived.

The time profiles of the gamma-ray emission recorded in different energy channels suggest the existence of three distinct intervals of the flare within the whole time interval under consideration (11:02:11 – 11:12:30 UT). We call these intervals A (from 11:02:11 to 11:03:40 UT), B (to 11:06:12 UT), and C (to 11:12:30 UT). The end of each previous interval coincides with the start of the following one. The subdivision of the flare into these

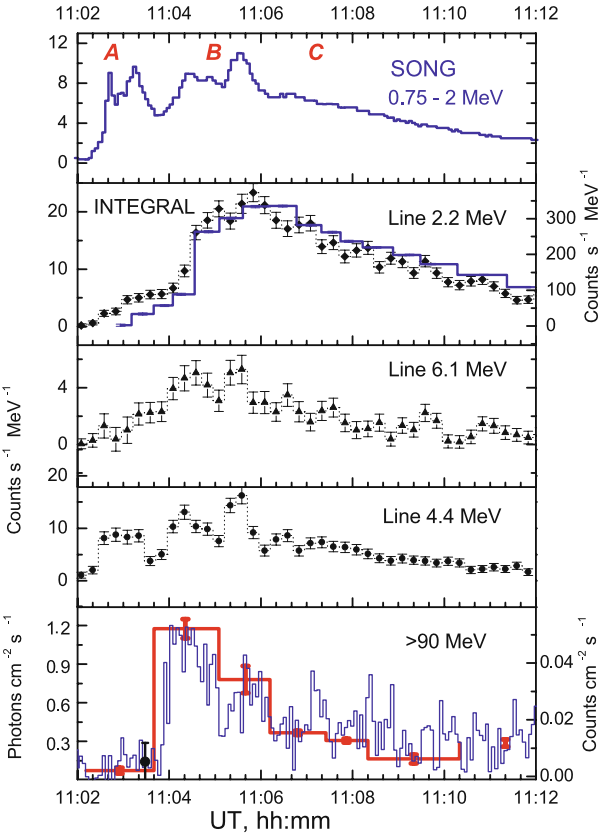

Figure 6 Time profiles of the gamma-ray emission produced by the flare of 28 October 2003. First (top) panel: SONG broad channels. For the definition of time intervals A, B, and C, see text. Second panel: the neutron-capture line measured by SONG (blue curve, left scale) and by INTEGRAL (diamonds, right scale; taken from Gros *et al.*, 2004). Third panel: de-excitation lines measured by INTEGRAL. Bottom panel: the SONG count rate at energies of > 90 MeV (blue curve, right scale) and the calculated pion-decay gamma-ray flux (red curve, left scale). Vertical dashed lines mark flare phases.

intervals can be justified directly by a comparison of the time behavior of count rates in different energy ranges (see Figure 5). Interval A corresponds to the strongest outburst in the channels from 2 – 6 MeV to 22.5 – 40 MeV. The onset of interval B is manifested as a jump in the count rate of the 90 – 150 MeV band with a statistical significance of 5σ at 11:03:51±2 s UT. We identify the transition between interval B and C from the fact that the count rates in all the SONG bands started to decay from 11:06 onwards. High-energy emissions lasted, at least, 530 s, with a weak variability during interval C. The same time intervals were identified from the time profiles of the nuclear de-exitation lines as well as the 2.223-MeV line emissions measured by INTEGRAL/SPI (Gros *et al.*, 2004; Kiener *et al.*, 2006). Trottet *et al.* (2008) identified these intervals by comparing the 210-GHz radio emission with SONG data.

In Figure 6 we present SONG data in a wide-band 0.75 – 2 MeV channel as well as at energies exceeding 90 MeV for a comparison with measurements of INTEGRAL/SPI (Gros *et al.*, 2004). Figure 6 also shows the time profile of the 2.223-MeV line emission recorded by SONG pulse-height analyzer with a time resolution of 30 s. The agreement between these time profiles verifies the accuracy of our measurements of the 2.223-MeV line emission.

One can see from Figure 6 that we have the following results.

i) The 4.4- and 6.1-MeV de-excitation line emission started during phase A.
ii) This emission increased suddenly at 11:04 ± 7 s UT, *i.e.*, practically at the same time as the $>$ 90-MeV emission did (11:03:51 ± 2 s UT). Later on, the de-excitation line

emission had basically the same time profile as the highest-energy > 90-MeV emission. The neutron-capture line emission was delayed, started at 11:04:41 UT, and reached a maximum at 11:06 UT. The temporal relation between different gamma-ray emissions produced by proton interactions implies either a significant hardening of the parent-proton spectrum during intervals B and C with respect to interval A, or a sharp increase of the number of accelerated particles, or both.

iii) The count rates in all low-energy broad SONG channels rapidly increased during interval B, simultaneously with a sharp rise of all gamma-ray line emissions and the high-energy > 90 MeV intensity.

3.2. The Dynamics of the Gamma-Ray Emission Spectrum

To clearly emphasize the difference between intervals A and B, we compared the count-rate spectra accumulated over these intervals (see Figure 7). The horizontal bars show the SONG energy ranges, and the vertical bars show the 1σ errors in the count rate. These spectra are quite different.

i) The count rate in the 0.23 – 2 MeV range increased during interval B with respect to interval A.

ii) The count rates in the 2 – 40 MeV range decreased in spite of a significant increase of the nuclear narrow de-excitation lines and neutron-capture line gamma emissions (see Figure 6), although they could provide some contribution to the count rate in the 2 – 10 MeV range of SONG channels. This means that the bremsstrahlung spectrum in the 0.2 – 40 MeV range becomes softer during phase B.

iii) The most important fact is that the spectral feature produced by the neutral-pion-decay emission appeared during interval B and dominated at energies above 40 MeV.

All of these facts support the idea that a new acceleration of both protons and electrons occurred at 11:03:51 ± 2 s UT.

For a quantitative analysis we selected seven successive time subintervals in the flare. Subinterval 1 started at 11:02:11 UT, interval 2 at 11:03:40 UT, interval 3 at 11:05:03 UT, interval 4 at 11:06:12 UT, interval 5 at 11:07:25 UT, interval 6 at 11:08:20 UT, and interval 7 started at 11:10:20 UT and ended at 11:12:20 UT. Subinterval 1 coincides with interval A

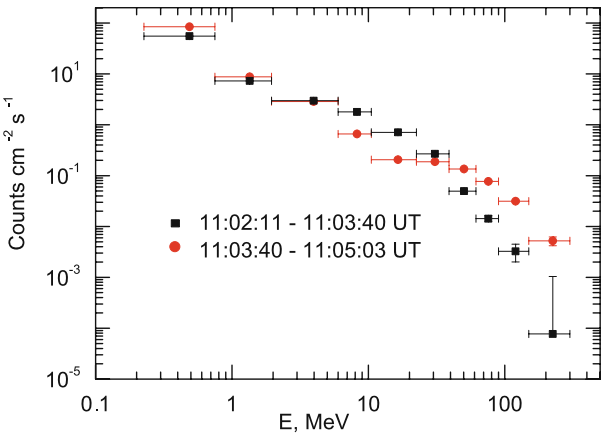

Figure 7 The count-rate spectra of the flare of 28 October 2003 recorded by SONG.

specified above; the sum of the second and third subintervals coincides with interval B, and the sum of intervals 4 – 7 coincides with interval C.

To restore the incident gamma-emission spectra we fitted the deposited count-rate spectra for selected time intervals with simulated deposited energy spectra prepared using the GEANT3.21 code. The corrected channel threshold values were used in this fitting. For the gamma-ray spectrum, we used a two-component model including a continuum component caused mainly by an electron bremsstrahlung and a pion-decay component in the form of a broad 'line' due to neutral-pion decay, peaking at 67 MeV, plus a continuum due to bremsstrahlung from electrons and positrons produced in charged pion decay (Murphy, Dermer, and Ramaty, 1987). Thus, the following form was chosen for the spectrum:

$$F(E) \propto w_c E^{-\gamma} C(E) + w_\pi \Phi(E) \tag{1}$$

Here, E is the photon energy, w_c and w_π are the weight coefficients of the components. The continuum component is represented by a power law with gradual steepening at high energies described by $C(E)$. The latter function was applied in two forms: as a power law with an index gradually changing with energy or as an exponential high-energy cutoff.

The spectral shape of the pion-decay component, $\Phi(E)$, from 0.2 to 2000 MeV was specially calculated for the flare of 28 October 2003 by R. Murphy (2010, private communication). It is similar to the commonly used spectra (Murphy, Dermer, and Ramaty, 1987). The pion-decay component in the case under consideration is produced by particles with a power-law energy spectrum extended to 10 GeV with a single slope $S = 3$, the α-proton ratio being 0.5. We assume an isotropic distribution in the hemisphere facing the solar photosphere (a 'downward isotropic' distribution). The location of the spectral maximum and the photon intensity in the energy range < 300 MeV are the same for the spectra at power-law slopes of both $S = 2$ and $S = 3$. We only use the pion-decay component that was calculated by R. Murphy for $S = 3$, since the highest-energy interval of SONG is 150 – 300 MeV.

The fitting procedure including the standard χ^2 permits us to calculate the pion-decay contribution and the total incident spectrum for each of the seven intervals. Table 2 contains time boundaries of selected intervals, estimated values of continuum emission index γ and calculated fluxes of gamma-ray emission at 1 and 100 MeV. The resulting incident spectra for intervals 1 and 2 are depicted in Figure 8.

Gamma-line emission could in principle additionally contribute to the count rates of the 0.75 – 10 MeV channels. Using the line fluxes found by INTEGRAL/SPI we find that the strongest lines will make only minor contributions in the broad SONG energy channels, compared to electron bremsstrahlung, and thus that de-excitation lines in the 1 – 7 MeV energy range will not significantly influence the parameters deduced for the power-law continuum spectral component. Kiener *et al.* (2006) also found that most counts in this energy range could be attributed to the continuum, apart from the fluxes in the 2.22, 4.44, and 6.13 MeV lines. On the other hand, the chosen shapes of the continuum spectra (a power law with a varying index or with an exponential cutoff) could adequately describe the possible deposit of these lines in the broad 2 – 10 MeV channels. We did not explicitly take into account these lines, simulating the response function, since our aim was not to describe in detail the continuum-and-line spectrum, which was a background for the pion-decay spectrum. To estimate additionally the actual contribution of the gamma-ray lines, we carried out a similar fitting using only the channels > 10 MeV, *i.e.* wittingly without the inclusion of these lines. Results of these fittings are similar, which verifies the negligible contribution of gamma lines to the spectra restored.

As mentioned above, the spectrum shape changes significantly during the development of the flare, which indicates the existence of at least two distinct flare intervals. Our analysis

Table 2 Gamma-ray fluxes and fluences for the flare of 28 October 2003.

Interval number	1	2	3	4	5	6	7
Start time (UT)	11:02:11	11:03:40	11:05:03	11:06:12	11:07:25	11:08:20	11:10:20
End time (UT)	11:03:40	11:05:03	11:06:12	11:07:25	11:08:20	11:10:20	11:12:20
γ	1.5	2.4	2.2	2.2	2.2	2.2	2.2
Gamma-ray flux at 1 MeV	18.0 ± 1.0	30.0 ± 1.0	32.0 ± 1.4	21.0 ± 1.0	20.0 ± 1.0	9.3 ± 1.0	5.0 ± 1.0
Gamma-ray flux at 100 MeV	$(2.2 \pm 0.5) \times 10^{-3}$	$(1.1 \pm 0.1) \times 10^{-2}$	$(7.5 \pm 0.9) \times 10^{-3}$	$(3.6 \pm 0.4) \times 10^{-3}$	$(2.9 \pm 0.3) \times 10^{-3}$	$(1.6 \pm 0.2) \times 10^{-3}$	$(2.7 \pm 0.2) \times 10^{-3}$
Gamma-ray fluence > 100 MeV	17 ± 4	260 ± 20	140 ± 20	70 ± 10	40 ± 4	50 ± 6	90 ± 8
Number of protons > 30 MeV	$< 1 \times 10^{32}$	$(3-8) \times 10^{32}$	$(3-4) \times 10^{32}$	$(1.5-1.9) \times 10^{32}$	$(0.9-1.1) \times 10^{32}$	$(1-1.3) \times 10^{32}$	$(1.9-2.2) \times 10^{32}$

Note: Flux units are photons $\mathrm{cm}^{-2}\ \mathrm{s}^{-1}\ \mathrm{MeV}^{-1}$, fluence units are photons cm^{-2}.

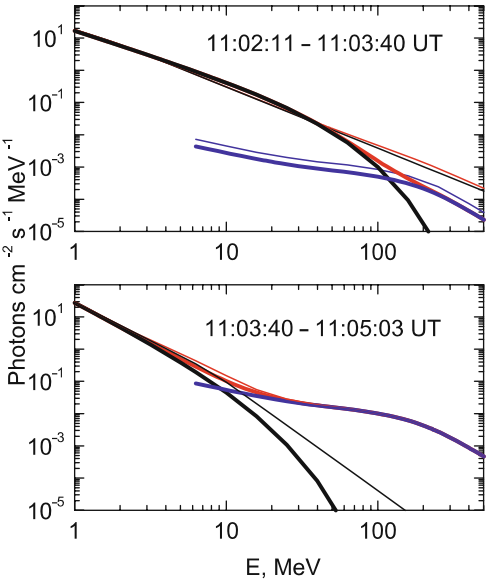

Figure 8 The incident gamma-ray spectra of the flare of 28 October 2003. Red curves represent the total spectra; black curves its continuum component; and blue curves the pion-decay gamma-ray spectrum. The thin curves correspond to a power law with varying index and the thick curves correspond to a power law with an exponential cutoff.

revealed that the spectrum of interval A represents a power-law continuum with a slope gradually changing with energy. The flux of the pion-decay emission at 100 MeV does not exceed $\sim 2.2 \times 10^{-3}$ photons cm^{-2} s^{-1} MeV^{-1}, irrespective of the choice of the trial spectrum. The contribution of this emission plays no significant role in the total photon fluxes at energies < 100 MeV. This suggests that the electrons were accelerated to at least 100 MeV. Some enhancement in de-excitation, positron annihilation, and neutron-capture gamma-ray lines' intensities can be seen in Figure 6, which is based on observations by INTEGRAL (Gros *et al.*, 2004) and SONG (in the 2.223 MeV line). This enhancement is caused by ions accelerated to 10 – 50 MeV/nucl during this phase.

Interval B was characterized by a remarkable plateau in the energy range of 60 – 300 MeV (see Figure 8). An analysis of the spectrum shape makes it clear that the high-energy emission in this interval is mainly due to the pion-decay component, which suggests that the acceleration of ions to energies > 300 MeV nucl^{-1} is more efficient than for interval A. At the same time, the bremsstrahlung spectrum became softer, and its index changed from 1.5 to 2.2 – 2.4 (see Table 2).

The time behavior of the neutral-pion-decay gamma-ray flux calculated from the spectrum fits is shown in the bottom panel of Figure 6. Note that the dynamics of this flux agrees well with the profile of the SONG count rates in the channels > 90 MeV, which allows us to regard this profile as a pion-production time profile. We note very sharp increases in both the pion-produced and the gamma-line emissions, which suggest that a new acceleration process began to operate during interval B. Interval C is characterized by a spectrum shape similar to that at interval B, differing from the latter only by a general decrease in gamma-ray emission.

3.3. Neutrons

Protons and nuclei accelerated to high energies and responsible for high-energy gamma-ray emission also produce high-energy neutrons through inelastic collisions in the solar atmosphere. These neutrons can escape the Sun and reach the Earth before their decay. The

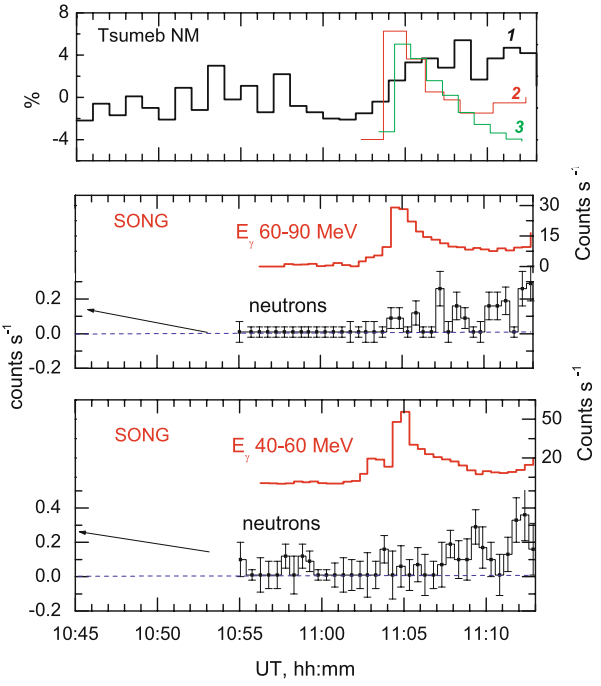

Figure 9 Solar-neutron observations on 28 October 2003. Upper panel: the black curve (1) corresponds to the Tsumeb NM data, the red line (2) corresponds to the gamma-ray flux with energies > 90 MeV measured by SONG (in arbitrary units), and the green line (3) to the neutron-emission profile (in arbitrary units) obtained by Bieber *et al.* (2005). Middle and bottom panels: the SONG data. The black curves represent the neutron count rates and the red curves correspond to the gamma-ray channels with the same energy deposit.

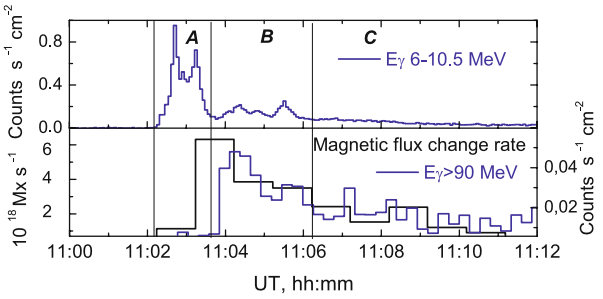

Figure 10 Time profiles of the gamma-ray emission measured by SONG during the flare of 28 October 2003 (blue curves) and the magnetic-flux change rate (from Miklenic, Veronig, and Vršnak, 2009b) (black curve).

28 October 2003 flare also provided clear signals of neutron production extending in energy to over 1 GeV with sufficient intensity to be recorded by SONG/CORONAS (Kuznetsov *et al.*, 2006a) and by neutron monitors at mountain altitudes.

The time behavior of the count rates in neutron channels with 40 – 60 and 60 – 90 MeV energy deposition is shown in Figure 9 in comparison with the gamma-ray channels having the same energy-deposition ranges. The admixture of photons is negligible in these neutron channels at the time of interest (see Figure 4). We found from our data that the onset of the solar-neutron event was between 11:06:20 and 11:07:10 UT. Tsumeb NM (19.2°S, 17.6°E, $H = 1240$ m, cutoff rigidity 9.29 GV) data are also presented in Figure 10. The Tsumeb NM enhancement to $3.4 \pm 0.3\%$ with its onset between 11:05 and 11:06 UT was claimed to result from solar-neutron flux (Plainaki *et al.*, 2005; Bieber *et al.*, 2005). There were also some uncertainties in the selection of neutron events by SONG and NM after the onset of the high-energy proton event at ∼ 11:12:30 UT.

Energetic (> 300 MeV) neutrons can be produced exclusively by protons and α-particles with energies not less than the energies of these neutrons themselves. An efficient acceleration of subrelativistic charged particles was observed only after 11:03:51 UT during flare intervals B and C, which is confirmed by an observation of the gamma-ray emission generated in neutral-pion decay. Figure 9 (upper panel) presents the time profile of this gamma-ray flux calculated from SONG data. This profile can be considered as a time profile of accelerated protons and, therefore, as the time profile illustrating the production of high-energy neutrons. It is similar to the best-fit profile for extended neutron emission at the Sun recalculated to 1 AU (Bieber *et al.*, 2005). This similarity reflects a common source of high-energy neutrons and pions, both being produced by high-energy protons.

The neutron energy cannot be directly measured by SONG because of the absence of an unambiguous relation between the incident-neutron energy and the secondary-particle energy deposited in the CsI(Tl) crystal. However, we can estimate the neutron energies comparing the onset time of the pion-decay emission with the onset time of the neutron event recorded by NM and SONG. The SONG neutron-flux onset (11:06:20 UT) corresponds to the highest neutron velocity, $v = 0.76c$ (≈ 550 MeV energy), and the NM onset (11:05 UT) corresponds to the upper limit of the neutron velocity, $v \approx 0.875c$ (≈ 1000 MeV). The lower energy threshold of NM for neutrons is 450 MeV due to the atmospheric absorption. The maximum of the SONG efficiency for neutrons corresponds to about 200 MeV, which can account for the difference in the measured time profiles.

4. Discussion and Results

We have presented X-ray and gamma-ray emissions from the 28 October 2003 solar flare as recorded by the SONG multi-channel detector onboard the CORONAS F satellite. The SONG data presented here have a 4-s time resolution and a sufficient energy resolution to yield unambiguous distinction of the pion-decay gamma-ray emission. SONG also detected high-energy neutrons. The SONG records provide unique information on the evolution of the flare electron and proton spectra.

Having processed the response of the SONG instrument to the emissions of the 28 October 2003 flare, we divided the first flare phase (usually called an impulsive phase) into two intervals, A and B. The bremsstrahlung generated by primary accelerated electrons dominated during interval A (from 11:02:11 to 11:03:40 UT) and extended up to 100 MeV. Protons accelerated to energies exceeding 10 MeV generated nuclear de-excitation gamma-ray lines and the 2.223-MeV line emission, which were recorded by SPI/INTEGRAL. During this interval, the pion-decay emission was absent or weak, *i.e.*, less than 2.2×10^{-3} photons $\mathrm{cm}^{-2}\,\mathrm{c}^{-1}\,\mathrm{MeV}^{-1}$ at 100 MeV. Interval B (from 11:03:40 to 11:06:12 UT) was characterized by a sharp increase of the gamma-ray line emission; moreover, emission produced by the decay of pion-decay gamma emission appeared as early as $11{:}03{:}51 \pm 2$ s UT. The increase of the high-energy emission was most likely due to interactions in the solar atmosphere of high-energy protons, a large number of which underwent strong acceleration up to energies exceeding 300 MeV. The maximum flux of the pion-decay emission reached 1.1×10^{-2} photons $\mathrm{cm}^{-2}\,\mathrm{s}^{-1}\,\mathrm{MeV}^{-1}$ at 100 MeV, exceeding all the fluxes that have ever been reported during the events: 3 June 1982 (Ramaty and Murphy, 1987), 15 June 1991 (Akimov *et al.*, 1991), 11 June 1991 (Dunphy *et al.*, 1999), 25 August 2001, 04 November 2003, 20 January 2005 (Kurt *et al.*, 2009, 2010).

Electrons also underwent an additional acceleration over a short timescale ($\sim 2-4$ s) at the beginning of interval B. The spectrum of the bremsstrahlung at energies > 10 MeV was

much steeper than the one obtained during interval A. During the long-duration interval C a decreasing pion-decay emission was also seen before the end of the observations.

Particularities of high-energy emissions from solar flares depend on the topological features of a particular flare site. Gamma-ray bursts similar to those registered in intervals A and B of the 28 October 2003 flare were also observed in the flares of 3 June 1982 (Chupp *et al.*, 1987), 24 May 1990 (Debrunner *et al.*, 1997; Vilmer *et al.*, 2003), 26 March 1991 (Akimov *et al.*, 1994), 25 August 2001 (Kurt *et al.*, 2009, 2010), 4 November 2003 (Kurt *et al.*, 2009, 2010), and 20 January 2005 (Kuznetsov *et al.*, 2006b, 2008a, Grechnev *et al.*, 2008). The durations of the first burst varied from 10 s (26 March 1991) to ~ 90 s (4 November 2003 and 20 January 2005). The first burst is caused mainly by high-energy electrons, whereas the second burst is characterized by efficient acceleration of protons to high energies. We think that the existence of these two distinct steps of particle acceleration is an intrinsic attribute of major flares.

At the same time a certain ambiguity in the phase separation was seen in major flares, and the transition between B and C intervals was not pronounced in several flares. The conventional identification of the flare phases based on the presence or absence of the pion-decay emission (see *e.g.* Chupp, 1996) does not seem to match the observations of the 28 October 2003 flare. Indeed, the commonly accepted terms of the 'impulsive phase' for the first phase with the predominance of bremsstrahlung and the 'extended phase' for a subsequent phase with pion-decay emission are unlikely to be appropriate, because either of these phases is impulsive. Only the C interval could be called 'the extended phase'. In particular, this 'extended phase' was clearly pronounced in the 11 and 15 June 1991 flares (Dunphy *et al.*, 1999, Akimov *et al.*, 1991, 1996), when the pion-decay emission was observed for several hours.

We have made an attempt to find the position of the acceleration process of high-energy protons on the time scale of the flare development using one of the observable consequences of the energy release in the corona. According to the most widely accepted model of erupting flares, the CSHKP model (Carmichael, 1964; Sturrock, 1966; Hirayama, 1974; Kopp and Pneuman, 1976), the bright, separating flare ribbons seen in UV bands chromospheric spectral lines, and prominent in Hα, are the chromospheric signatures of the energy release in the corona. The energy, which has been released at the primary energy-release site, is transported downward into the chromosphere along the newly reconnected field lines by fast particles and the thermal conduction. When it is deposited at the two foot-points of the field lines, which are rooted inside opposite magnetic polarities, the chromosphere brightens, and so-called flare kernels are created. Image time-series which measured newly brightened flare area and magnetic-field strength inside this area, when the flare is in progress, allow one to calculate the cumulated positive and negative magnetic flux participating in the reconnection process.

Miklenic, Veronig, and Vršnak (2009a, 2009b) inferred the flare magnetic reconnection rate in the form of the magnetic-flux change rate for several flares using SOHO/MDI magnetogram, and high-cadence Hα and TRACE 1600 Å image time-series. A similar analysis was provided by Li *et al.* (2009) with HINODE/SOT data for the 16 December 2006 flare. In all these events the reconnection rate correlates more or less in time with the electron bremsstrahlung and microwave emission, indicating a physical link between the flare magnetic reconnection and the acceleration of non-thermal electrons.

We compared the derived magnetic-flux change rate for the 28 October 2003 flare (Miklenic, Veronig, and Vršnak, 2009b) with the SONG observations of non-thermal emissions. Figure 10 presents the magnetic-flux change rate combined with the gamma-emission count rate in the 6 – 10.5 MeV channel created by high-energy electrons and with count rate, averaged over 16 s, above 90 MeV, generated by protons with energies > 300 MeV.

The sharp increase of pion-decay emission that occurred at 11:03:51 ± 2 s UT is going on during the 11:03:12 – 11:04:12 UT time interval, which is the first bin of the sharp rise of magnetic-flux change rate. Thereafter a strong temporal correlation between the derived magnetic-flux change rate and the observed pion-decay emission was seen. On the other hand, the burst of gamma-ray emission detected during phase A and caused by electrons was observed when the reconnection flux was small. So we are faced with the fact that the most efficient acceleration of high-energy proton during the impulsive phase of this flare coincides in time with the highest rate of the magnetic-flux change rate. Unfortunately, data of the magnetic field have ∼ 1 min. time cadence, which does not allow us to make a more accurate comparison.

The knowledge of the gamma-ray fluences measured in the marked energy ranges (the neutron-capture line emission, $F_{2.2}$; the nuclear line emission in the range 4 – 7 MeV, F_{4-7}; and the neutral-pion-decay gamma-ray emission at 100 MeV, $F_{\pi 0}$) makes it possible to estimate the energy spectrum shape of solar protons responsible for the production of these emissions (see *e.g.* Murphy and Ramaty, 1984; Ramaty and Murphy, 1987; Murphy, Dermer, and Ramaty, 1987; Ramaty *et al.*, 1993; Dunphy *et al.*, 1999). In particular, the ratio of the fluences $F_{2.2}$ and F_{4-7} can be used to estimate the proton spectrum in the energy range of 10 – 30 MeV, and the ratio of F_{4-7} to $F_{\pi 0}$ yields similar information on the spectrum in the range of 30 – 300 MeV. The latter ratio depends strongly on the shape of the spectrum of accelerated particles and differs substantially in the cases of power-law or exponential spectra.

We calculated the fluences of the neutral-pion-decay component using the best-fit spectral parameters of the gamma-ray emission obtained for each interval of the 28 October 2003 flare (see Table 2). The value of F_{4-7} was taken to be equal to the sum of the 4.4 and 6.1 MeV lines (Kiener *et al.*, 2006), because a possible contribution from other lines in this range was not important in this flare and could not significantly affect the $F_{4-7}/F_{\pi 0}$ ratio. To roughly estimate the shape of the proton spectrum, we employed the procedure used by Dunphy *et al.* (1999) for a power-law spectrum. We used Figure 4 from that paper to find the relevant ratios $F_{\pi 0}/F_{4-7}$ as a function of the proton-spectrum shape. Two patterns of proton distribution with respect to the solar surface are typically considered, *viz.*, a 'horizontal' distribution and a distribution 'isotropical in the downward hemisphere' (Ramaty *et al.*, 1993). We used the second pattern because Kiener *et al.* (2006) found narrow, downward directed particle beams perpendicular to the solar surface to clearly favor both the B and C intervals.

Figure 4 from Dunphy *et al.* (1999) demonstrates that the value of the power-law index of the proton spectrum depends on the fluence ratio in such a way that the variation of this ratio by a factor of three leads to variations of the power-law index which do not exceed 10%. So the possible errors of detector calibrations are of minor importance.

The experimental data within their accuracy along with the theoretical curve lead us to conclude that the features of intervals B and C appear to be consistent with a power-law spectrum. This spectrum index is constant or changes within the estimation error ($S \sim 3 \pm 0.4$). On the other hand, Kiener *et al.* (2006) found a power-law spectrum of $3 < S < 4$ from the $F_{2.2}/F_{4-7}$ ratio for intervals B and C. In the same way, Share *et al.* (2004) found $S \approx 3.4$ for the extended phase after 11:06 UT. Thus, the data sets available for intervals B and C are consistent with a power-law spectrum with an index ($S = 3 - 3.5$) that varies weakly, if at all, over the energy range of 10 – 300 MeV. The coincidence of the obtained slope of the proton spectrum with the index used in our fitting routine ($S = 3$) is not crucial because the dependence of the pion-decay emission spectrum on the parent-proton spectrum is weak in this energy range. On the other hand, the spectral slope of the solar particles in the energy range 0.5 – 10 GeV measured for this event by NMs was found to be ∼ 3.5

(Miroshnichenko *et al.*, 2005). Kuznetsov *et al.* (2008b) obtained a similar value for the proton-spectrum slope from CORONAS-F data using the effect of a geomagnetic cutoff. We may guess that close agreement between these values and the spectral slope derived from the gamma-ray measurements is not coincidental but reflects a common origin of the accelerated and escaping protons.

Values obtained of gamma-ray fluences combined with the proton-spectrum index allow one to estimate the total number of interacting particles with energies > 30 MeV. These figures, calculated for selected intervals under the assumption of $S = 3$ and of isotropic angle distribution of gamma-rays (Ramaty and Murphy, 1987), are listed in Table 2. Note that the total number of interacting particles depends strongly on the chosen fitting model and its parameters (see, *e.g.*, Murphy, Dermer, and Ramaty, 1987; Vilmer *et al.*, 2003), in particular on the maximum ion energy attained. However, Vilmer *et al.* (2003) indicate a weak dependence of fast proton numbers on the upper cutoff of the parent-proton spectrum if this cutoff exceeds 2000 MeV, as was in the case under consideration.

Another important property of this flare was the observed primary-electron bremsstrahlung, which was not mimicked by pion-produced gamma rays during interval A (see Figure 8). Thus, electrons were accelerated during this phase up to, at least, 100 MeV. At later stages, gamma rays produced in the pion decay dominated. This makes estimations of the upper energy of accelerated electrons during interval B difficult. We recall that gamma-ray emission with energies of up to 300 MeV was recorded during the flare of 26 March 1991 (Akimov *et al.*, 1994). The spectrum of that flare could be described by a single power law with an index of three and did not contain any contribution of the pion-decay emission, *i.e.*, it was entirely due to electron bremsstrahlung.

The appearance of high-energy protons during the flare is evidenced by the commencement of the pion-decay component, which is recognized with an accuracy of a few seconds. We emphasize that just the detection of the gamma-ray emission produced by the decay of neutral pions provides the most accurate and direct way to determine, at least, the onset of the proton acceleration to hundreds of MeV and higher energy, because no other process does exist which could imitate the corresponding spectral feature. Other methods used to determine when the acceleration of heavy particles started (analyses of radio emission, the motion of CMEs, the arrival times of particles at Earth) are all indirect; they provide ambiguous results, which sometimes contradict each other.

The time profiles and spectral characteristics of gamma emission deduced in the A, B, and C intervals as well as the strong correlation between pion-decay flux (proton production) and magnetic-flux change rate imply that acceleration of high-energy protons and of relativistic electrons is an intrinsic property of the impulsive energy-release process; and they appear to be important for particle acceleration models.

Acknowledgements We are deeply indebted to G. Share, V.V. Akimov, I.N. Myagkova, and V.V. Grechnev for discussions, to R. Murphy for providing calculated pion-decay spectra, to C. Miklenic for data on the magnetic-flux change rate and to the anonymous reviewers for useful comments. This work was supported by the Russian Foundation for Basic Research (project 09-02-01145). KK wishes to acknowledge VEGA agency (project VEGA 2/0081/10) for support.

References

Akimov, V.V., Afanassyev, V.G., Belaousov, A.S., Blokhintsev, I.D., Kalinkin, L.F., Leikov, N.G., *et al.*: 1991, In: *Proc. 22nd Int. Cosmic Ray Conf.*, **3**, 73.

Akimov, V.V., Leikov, N.G., Kurt, V.G., Chertok, I.M.: 1994, In: Ryan, J.M., Vestrand, W.T. (eds.) *High Energy Solar Phenomena*, AIP, New York, 130.

Akimov, V.V., Ambroz, P., Belov, A.V., Berlicki, A., Chertok, I.M., Karlicky, M., Kurt, V., Leikov, N., Litvinenko, Yu., Magun, A., Minko-Wasiluk, A., Rompolt, B., Somov, B.: 1996, *Solar Phys.* **166**, 107.
Bieber, J.W., Clem, J., Evenson, P., Pyle, R., Ruffolo, D., Saiz, A.: 2005, *Geophys. Res. Lett.*, **32**, L03S02.
Bogomolov, A.V., Britvich, G.I., Myagkova, I.N., Ryumin, S.P.: 1996, *Instrum. Exp. Tech. (USA)* **39**, 1.
Bogomolov, A.V., Ignat'ev, A.P., Kudela, K., Kuznetsov, S.N., Logachev, Yu.I., Morozov, O.V., Myagkova, I.N., Oparin, S.N., Pertsov, A.A., Svertilov, S.I., Yushkov, B.Yu.: 2003, *Astron. Lett. (Russia)* **29**, 199.
Carmichael, H.: 1964, In: Hess, W.N. (ed.) *The Physics of Solar Flares*, NASA, Washington, 451.
Chupp, E.L., Debrunner, H., Flückiger, E., Forrest, D.J., Golliez, F., Kanbach, G., Vestrand, W.T., Cooper, J., Share, G.: 1987, *Astrophys. J* **318**, 913.
Chupp, E.L.: 1996, In: Ramaty, R., Mandzhavidze, N., Hua, X.-M. (eds.) *High Energy Solar Physics*, AIP, New York, 3.
Debrunner, H., Flückiger, E., Chupp, E.L., Forrest, D.J.: 1983, In: *Proc. 18th Int. Cosmic Ray Conf.*, **4**, 75.
Debrunner, H., Lockwood, J.A., Barat, C., Bütikofer, R., Dezalay, J.P., Flückiger, E., Kuznetsov, A., Ryan, J.M., Sunyaev, R., Terekhov, A., Trottet, G., Vilmer, N.: 1997, *Astrophys. J.* **479**, 997.
Dunphy, P.P., Chupp, E.L., Bertsch, D.L., Schneid, E.J., Gottesman, S.R., Kanbach, G.: 1999, *Solar Phys.* **187**, 45.
Forrest, D.J., Vestrand, W.T., Chupp, E.L., Rieger, E., Cooper, J., Share, G.H.: 1985, In: *Proc. 19th Int. Cosmic Ray Conf.*, **4**, 146.
Grechnev, V.V., Kurt, V.G., Chertok, I.M., Uralov, A.M., Nakajima, H., Altyntsev, A.T., Belov, A.V., Yushkov, B.Yu., Kuznetsov, S.N., Kashapova, L.K., Meshalkina, N.S., Prestage, N.P.: 2008, *Solar Phys.* **252**, 149.
Gros, M., Tatischeff, V., Kiener, J., Cordier, B., Chapius, C., Weidenspointner, G., Vedrenne, G., von Kienlin, A., Diehl, R., Bykov, A., Mendez, M.: 2004, In: Schonfelder, V., Lichti, G., Winkler, C. (eds.) *Proc. 5th INTEGRAL Workshop*, *ESA* **SP-552**, 669.
Harris, M.J., Share, G.H., Leising, M.D.: 2003, *J. Geophys. Res.* **108**(A12), 1435.
Hirayama, T.: 1974, *Solar Phys.* **34**, 323.
Kiener, J., Gros, M., Tatischeff, V., Weidenspointner, G.: 2006, *Astron. Astrophys.* **445**, 725.
Kopp, R.A., Pneuman, G.W.: 1976, *Solar Phys.* **50**, 85.
Kurt, V.G., Akimov, V.V., Leikov, N.G.: 1996, In: Ramaty, R., Mandzhavidze, N., Hua, X.-M. (eds.) *High Energy Solar Physics*, AIP, New York, 237.
Kurt, V.G., Yushkov, B.Yu., Kudela, K., Galkin, V.I.: 2009, In: *Proc. 31st Int. Cosmic Ray Conf.*, paper 0589.
Kurt, V.G., Yushkov, B.Yu., Kudela, K., Galkin, V.I.: 2010, *Cosmic Res.* **48**, 70.
Kuznetsov, S.N., Kudela, K., Ryumin, S.P., Gotselyuk, Yu.V.: 2002, *Adv. Space Res.* **30**, 1857.
Kuznetsov, S.N., Kudela, K., Myagkova, I.N., Yushkov, B.Yu.: 2003a, In: *Proc. 28th Int. Cosmic Ray Conf.*, 3183.
Kuznetsov, S.N., Kudela, K., Myagkova, I.N., Yushkov, B.Yu.: 2003b, In: Wilson, A. (ed.) *Proc. ISCS 2003 Symp.*, *ESA* **SP-535**, 683.
Kuznetsov, S., Kudela, K., Myagkova, I., Podorolskiy, A., Ryumin, S., Yushkov, B.: 2004, *Indian J. Radio Space Phys.* **33**, 353.
Kuznetsov, S., Kurt, V., Yushkov, B., Myagkova, I., Kudela, K., Belov, A., Caroubalos, C., Hilaris, A., Mavromichalaki, H., Moussas, X., Preka-Papadema, P.: 2005a, *Int. J. Modern Phys. A* **20**, 6705.
Kuznetsov, S.N., Yushkov, B.Yu., Kudela, K., Myagkova, I.N., Starostin, L.I., Denisov, Yu.I.: 2005b, *Adv. Space Res.* **36**, 1997.
Kuznetsov, S.N., Kurt, V.G., Myagkova, I.N., Yushkov, B.Yu., Kudela, K.: 2006a, *Solar System Res.* **40**, 104.
Kuznetsov, S.N., Kurt, V.G., Yushkov, B.Yu., Kudela, K.: 2006b, *Bull. Russ. Acad. Sci. Phys.* **70**, 1665.
Kuznetsov, S.N., Kurt, V.G., Yushkov, B.Yu., Kudela, K.: 2008a, In: *Proc. 30th Int. Cosmic Ray Conf.*, **1**, 121.
Kuznetsov, S.N., Yushkov, B.Yu., Kudela, K., Bucik, R.: 2008b, In: *Proc. 30th Int. Cosmic Ray Conf.*, **1**, 71.
Li, C., Dai, Y., Vial, J.-C., Owen, C.J., Matthews, S.A., Tang, Y.H., Fang, C., Fazakerley, A.N.: 2009, *Astron. Astrophys.*, **503**, 1013.
Mewaldt, R.A., Cohen, C.M.S., Labrador, A.W., Leske, R.A., Mason, G.M., Desai, M.I., Looper, M.D., Mazur, J.E., Selesnick, R.S., Haggerty, D.K.: 2005, *J. Geophys. Res.* **110**, A09S18.
Miklenic, C.H., Veronig, A.M., Vršnak, B.: 2009a, *Cent. Eur. Astrophys. Bull.*, **33**(1), 197.
Miklenic, C.H., Veronig, A.M., Vršnak, B.: 2009b, *Astron. Astrophys.* **499**, 893.
Miroshnichenko, L.I., Klein, K.-L., Trottet, G., Lantos, P., Vashenyuk, E.V., Balabin, Y.V., Gvozdevsky, B.B.: 2005, *J. Geophys. Res.* **110**, A09S08.
Murphy, R.J., Ramaty, R.: 1984, *Adv. Space Res.* **4**, 127.
Murphy, R.J., Dermer, C.D., Ramaty, R.: 1987, *Astrophys. J. Suppl.* **63**, 721.
Nonaka, T., Hayashi, Y., Ito, N., Kawakami, S., Matsuyama, T., Oshima, A., Tanaka, H., Yoshikoshi, T., Gupta, S.K., Jain, A., Karthikeyan, S., Mohanty, P.K., Morris, S.D., Rao, B.S., Ravindran, K.C., Sivaprasad, K., Sreekantan, B.V., Tonwar, S.C., Viswanthan, K., Kojima, H.: 2006, *Phys. Rev. D* **74**, 052003.

Panasyuk, M.I., Bogomolov, A.V., Germantsev, Yu.L., Kudryavtsev, M.I., Kuzhevsky, B.M., Kuznetsov, S.N., Lyagushin, V.I., Myagkova, I.N., Ryumin, S.P., Shavrin, P.I., Sobolevsky, N., Svertilov, S.I., Yushkov, B.Yu.: 2001, In: *RADECS 2000 Workshop Proc.*, Univ. Catholique Louvain, Belgium, 9.
Plainaki, C., Belov, A., Eroshenko, E., Kurt, V., Mavromichalaki, H., Yanke, V.: 2005, *Adv. Space Res.* **35**, 691.
Ramaty, R., Murphy, R.J.: 1987, *Space Sci. Rev.* **45**, 213.
Ramaty, R., Mandzhavidze, N., Kozlovsky, B., Skibo, J.G.: 1993, *Adv. Space Res.* **13**, 275.
Rieger, E.: 1989, *Solar Phys.* **121**, 323.
Share, G.H., Murphy, R.J., Smith, D.M., Schwartz, R.A., Lin, R.P.: 2004, *Astrophys. J. Lett.* **615**, 169.
Sturrock, P.A.: 1966, *Nature* **211**, 695.
Trottet, G., Krucker, S., Lüthi, T., Magun, A.: 2008, *Astrophys. J.* **678**, 509.
Veselovsky, I.S., *et al.*: 2004, *Cosmic Res.* **42**, 433.
Vilmer, N., MacKinnon, A.L., Trottet, G., Barat, C.: 2003, *Astron. Astrophys.* **412**, 865.